ELSEVIER

Journal of Volcanology and Geothermal Research 91 (1999) 79–96

Journal of volcanology and geothermal research

www.elsevier.com/locate/jvolgeores

Dielectric constant as a predictor of porosity in dry volcanic rocks

A.C. Rust *, J.K. Russell, R.J. Knight

Department of Earth and Ocean Sciences, University of British Columbia, Vancouver, B.C., Canada V6T 1Z4

Received 20 May 1998; accepted 20 April 1999

Abstract

Measurements of dielectric constant (K') are made on 34 samples of volcanic rocks at frequencies of 0.01 to 10 MHz under ambient atmospheric conditions. Bulk density (ρ_T), total porosity (Φ_T) and connected porosity (Φ_{Conn}) are also measured. The samples derive from two dacitic lava flows (~60–62 and 68 wt.% SiO_2), dacitic pyroclastic deposits (~66–68 wt.% SiO_2) and two basalt lava flows (~49–52 wt.% SiO_2). Each locality provided a suite of samples with similar mineralogy and composition but a range of porosities. Porosity measurements indicate that as much as 17% of pumice pore space can be unconnected. The data show a strong correlation between K' and Φ_T and the dacitic rocks show a 2.5-fold decrease in K' over a porosity range of 8–79%. The data are fitted to a time propagation (TP) model and to a more general two-parameter model based on the Lichtenecker–Rother equation. For dacitic rocks, the dielectric constant is best related to porosity by:

$$(K')^{0.96} = \Phi + 6.51(1 - \Phi).$$

K' and ρ_T are also strongly correlated in these sample sets. The trend formed by samples of dacite in (K', ρ_T) space is linear and the data compare well with published values for other non-basaltic rocks. Samples of basalt show greater variance in measured values of K', due perhaps to higher and more variable modes of Fe–Ti oxide minerals. These new data suggest the possibility of inverting radar velocity data to obtain estimates of porosity in dry volcanic successions. Inversion of radar data for porosity could be useful in discriminating between units of an eruption cycle (e.g., lava flow, pyroclastic flow, airfall) and mapping porosity variations within deposits such as welded pyroclastic flows.

Keywords: porosity; dielectric constant; density; volcanic rocks; GPR

1. Introduction

Ground penetrating radar (GPR) is a high-resolution, near-surface, geophysical technique that can be used to image geological structures and materials in the subsurface. Young volcanic deposits are ideal candidates for GPR surveys because they are electrically resistive, and commonly form thin (< 50 m) surficial deposits. Of specific interest in our research is the use of GPR to obtain information on the spatial variability of porosity in young volcanic deposits. Such information is critical to volcanology because volcanic rocks are commonly vesicular and can show large variations in porosity that relate directly to process.

* Corresponding author

0377-0273/99/$ - see front matter
PII: S0377-0273(99)00055-4

Information about material properties of the subsurface can be extracted from GPR data by obtaining estimates of radar velocities. This is done using common midpoint surveys, which employ an acquisition geometry that makes it possible to determine the velocity with which an electromagnetic wave travels through a region of the subsurface. The dielectric constant (K') of the material in the region can be calculated from the velocity. However, the conversion of K' into material properties, such as porosity, requires an understanding of the dielectric properties of volcanic rocks. Knowledge of the factors contributing to K' of volcanic deposits also impacts our ability to predict what aspects of volcanic deposits can best be imaged with GPR.

The relationship between the measured dielectric properties and the porosity of volcanic rocks is affected by numerous factors such as mineralogy, water content, and phase geometries, thus making the accurate interpretation of porosity from GPR data a challenging research problem. In this study, we begin to address this issue by investigating the dependence of K' on porosity for dry volcanic rocks. Measurements of K' are presented for several compositions of volcanic rocks over a range of porosities, and a model is presented that relates porosity to dielectric constant. Our model represents a first step towards using GPR data to both image and quantify porosity variation in young volcanic deposits.

2. Previous studies

Table 1 summarizes the results of 24 papers reporting dielectric constant measurements of igneous rocks and includes information on samples, methodology and additional physical properties. The dielectric properties of igneous rocks, and volcanic rocks in particular, have been shown to be sensitive to frequency and temperature (e.g., Chung et al., 1970; Saint-Amant and Strangway, 1970), water saturation (Roberts and Lin, 1997), mineralogy (e.g., Hansen et al., 1973), fabric (Tuck and Stacey, 1978; Hawton and Borradaile, 1989), and bulk density (e.g., Olhoeft and Strangway, 1975). Bulk density is strongly affected by porosity changes but, to date, there has been no systematic analysis of the relationship between porosity and dielectric constant for volcanic rocks.

2.1. Density and K'

Measurements of density and K' have been made on rocks and their corresponding powders (Campbell and Ulrichs, 1969; Troitsky and Shmulevich, 1973; Frisnillo et al., 1975), on suites of solid and/or naturally unconsolidated volcanic rocks (Chung et al., 1970; Gold et al., 1971, 1973), on solid rocks (Bondarenko, 1971; Shmulevich et al., 1971) and on unconsolidated material (Gold et al., 1970; Adams et al., 1996).

The most comprehensive study in terms of the range of density and the range of chemical compositions of volcanic rock samples is by Shmulevich et al. (1971). They measured the dielectric properties of 89 acidic to ultrabasic igneous rocks (68 volcanic, 21 intrusive) at a frequency of 500 MHz. As with most studies that measured dielectric constant against density (Table 1) they report only values of bulk density (ρ_T: total density of rock including voids) and not solid density (ρ_S: void-free density). The bulk density (ρ_T) of volcanic samples ranged from 0.54 to 2.90 g/cm^3. Rather than compare ρ_T and K' directly, Shmulevich et al. (1971) plotted K' and the Krotikov parameter (a), against SiO_2 content. The Krotikov parameter is defined as:

$$a = \sqrt{K'} - 1/\rho_T \quad (1)$$

Troitsky and Shmulevich (1973) found the Krotikov parameter to be practically invariant for lower density igneous rocks ($\rho_T \leq 2$ g/cm^3), and for all acidic rocks, regardless of density. This study and others (e.g., Campbell and Ulrichs, 1969; Adams et al., 1996) indicate a trend of increasing K' with decreasing SiO_2 content of volcanic rocks.

Using the values of a and ρ_T reported by Shmulevich et al. (1971), we have recalculated values of K'. Fig. 1 is a plot comparing the values of K' and ρ_T (Shmulevich et al., 1971) against model curves of Olhoeft and Strangway (1975) and Ulaby et al. (1990). Ulaby et al. (1990) fit experimental data from 80 rocks of diverse origin (volcanic, plutonic, clastic, carbonate and 'other') to:

$$K' = (1.96 \pm 0.14)^{\rho_T} \quad (2)$$

Their dielectric data were collected at frequencies from 0.5 to 18 GHz. K' was found to be indepen-

dent of frequency and they attributed 50% of the variance in the data to variations in sample density. Olhoeft and Strangway (1975) compiled and fit density measurements (92 solid and unconsolidated lunar rocks) to values of K' measured at frequencies greater than 0.1 MHz. Their model curve (Eq. (3)) is very similar to that of Ulaby et al. (1990):

$$K' = (1.93 \pm 0.17)^{\rho_T} \quad (3)$$

The K' predicted by the models of Olhoeft and Strangway (1975) and Ulaby et al. (1990) are consistently lower than the majority of the data of Shmulevich et al. (1971). Although intended to predict dielectric constant as a function of ρ_T over the complete range of densities, the models describe the lower density (< 2.0 g/cm^3) data best. The discordance between the model and measured values of K' increases markedly at higher values of bulk density (Fig. 1) which suggests the presence of another control. Nevertheless, density is a good predictor of dielectric constant for volcanic rocks of low to moderate density.

2.2. Porosity and K'

There are few published data relating dielectric constant directly to porosity (Φ) for volcanic rocks. Five studies by Campbell and Ulrichs (1969), Chung et al. (1970), Gold et al. (1970), Adams et al. (1996) and Russell and Stasiuk (1997) provide a total of 28 (Φ, K') points (Fig. 2). Data from Drury (1978) and Roberts and Lin (1997) are omitted because the samples were saturated with fresh water or seawater (Table 1). Measurements of K' were made at a variety of frequencies, and compositions of samples, states of consolidation and methods of measuring porosity all varied.

Campbell and Ulrichs (1969) and Gold et al. (1970) used powdered samples and porosity was calculated assuming that the rock from which the powder originated was not porous (i.e., $\rho_{T(rock)} = \rho_{S(rock)} = \rho_{S(powder)}$):

$$\Phi_{T(powder)} = 1 - \frac{\rho_{T(powder)}}{\rho_{T(rock)}} \quad (4)$$

Thus, the reported values of porosity represent minima; the extent to which they are low depends on the actual porosity of the original rocks. The four data points from Gold et al. (1970) derive from a single powdered lunar rock compacted to various porosities. The eleven data points from Campbell and Ulrichs (1969) represent crushed rocks of different composition: obsidian (2), trachyte, phonolite, and basalt (7). All powders were compacted to a porosity of 40%. One objective of this study (Campbell and Ulrichs, 1969) was to compare the electrical properties of powdered material to those of the corresponding rock. They found that the difference in K' between rock types was much smaller where measured on powdered rocks (all at 40% porosity) relative to measurements on the solid rock equivalents.

The relevant samples of Adams et al. (1996) consist of six natural volcanic ashes of variable composition (basalt (2), andesite, dacite (2), and rhyolite) and two powdered basalt samples. K' measurements were made from 4 to 19 GHz. Porosity and density values themselves are not reported but rather the fractional volumes (e.g., $\rho_{T(powder)}/\rho_S$) are listed. However, Adams et al. (1996) do not state how the solid densities were determined. Fractional volume is equivalent to $1 - \Phi$ and the relationship between Φ and K' was indirectly explored by testing the validity of various mixing formulas in relating the dielectric constants of porous powders to the dielectric constants of their solid rock equivalents.

Russell and Stasiuk (1997) measured dielectric constants of four volcanic rocks (basalt lava, dacite pumice, dense obsidian breccia, and dacite lava). They argued that sample porosity is primarily responsible for variations in K', implying that chemical composition, modal mineralogy, proportion of glass, and grain size have only secondary effects. Measurements were made on multiple sub-samples of each of the four hand-samples. Two of the rock types (basalt and pumice) showed significant variance in K'. Although there was not always a clear relationship between porosity (determined with a helium pycnometer) and dielectric constant in sub-sample suites, a direct correlation was found between the relative variance in sample porosity and the variation in dielectric properties between disks taken from the same hand-sample.

The data point from Chung et al. (1970) is from a lunar rock of unusual chemistry (Kanamori et al., 1970) with low silica (37 wt.% SiO_2) and very high

Table 1
Details of 24 previous studies that report dielectric constant measurements on igneous samples

Samples		K' measurement				Other properties[a]		Source[b]
Material	State[c]	Frequency	Geometry[d]	Coating	Moisture condition			
Volcanic ash; basalt; granite	u; s; p	4–19 GHz	n.a.	–	dry; ambient[e]	Φ	X, $\tan\delta$	1
Plutonic rocks	s	5 kHz	disks: d = 10–12 mm, h = 2–3 mm	Pt-foil	dry; ambient[e]	ρ	P, T	2
Igneous rocks	s; p	0.45 and 35 GHz	parallelepipeds: $0.71 \times 0.36 \times 0.25$ cm^3	–	ambient[e]	ρ	X, T, l_a, $\tan\delta$	3
Basalt; gabbro; lunar rocks (real and simulated)	s	100 Hz–10 MHz	parallelepipeds	tin foil	pre-dried in 150°C vacuum	ρ,Φ(1)	X, T, $\tan\delta$, σ	4
Basalt	s	1 Hz–1 MHz	disks: d = 2.54 cm, h = 0.5–1.0 cm	–	seawater-saturated	Φ	$\tan\delta$, σ	5
Lunar soils; basalt	u; s	0.2–100 kHz	n.a.	–	dry; measured in vacuum	ρ	(X), P, $\tan\delta$	6
Lunar rocks and soils	s; u	450 MHz	n.a.	–	ambient[e]; dried in vacuum oven	ρ, Φ	(X), $\tan\delta$, R, p, l_a	7, 8, 9
Basalt; lucite and ilmenite powders	s; p	100 Hz–50 MHz	n.a.	–	dry nitrogen atmosphere; ambient for powders		X, $\tan\delta$	10
Metavolcanics	s	5 Hz–13 MHz	disks: d = 12.2 mm, h = 2 mm	–	20%, 45% relative humidity		$\tan\delta$, strain anisotropy	11
Obsidian; plutonic rocks	s	50 Hz–30 MHz	disks: d = 2.2–5.1, h = 0.1–0.4 cm	Ag paint; Sn–Pb foil and petroleum	dry and moist; under vacuum and in air			12
Lunar rocks and soils	s; u	variable	variable	–	ambient[e]	ρ	X, $\tan\delta$	13
Lunar soil	u	100 Hz–1 MHz	–	–	dry; under vacuum		T, (X), σ	14
Rhyolite tuff	s	0.1–100 kHz	disks: d = 5.1 cm, h = 2, 3, 4, 5 mm	Au sputter; Au foil	variable water saturation	ρ, Φ	T, $\tan\delta$, σ	15
Basalt; dacite	s	10 Hz–10 MHz	disks: d = 5 cm, h = 0.5 cm	Au sputter	ambient	Φ	(X)	16
Dunite; basalt	s; p	50 Hz–2 MHz	disks: $h \sim 2$ mm	–	dry; under vacuum		T, $\tan\delta$	17
Igneous rocks	s	500 MHz	n.a.	–	ambient[e]	ρ	X, $\tan\delta$, σ	18
Igneous rocks	p	0.545–37.5 GHz	–	–	ambient[e]		T, $\tan\delta$	19
Igneous rocks	s	0.1–20 MHz	slabs: t = 0.4–1.1 cm	–	dry and wet (up to 6.4%) moisture			20
Lunar soils; granite	s; u	0.1–100 kHz	n.a.	–	dry, under vacuum and in air		T, (X), σ, l_a	21
Volcanic rocks; granite; peridotite	p	9.4 GHz	–	–	ambient[e]	ρ	$\tan\delta$	22
Basalt	s	2.3 kHz	disks: d = 16 mm, $h \sim 14$ mm	–	dry; cell flushed with dried air before measurement		magnetic anisotropy	23
Igneous rocks	s	0.5–18 GHz	$t > 4$ mm	–	dry; ambient[e]	ρ	X, $\tan\delta$	24

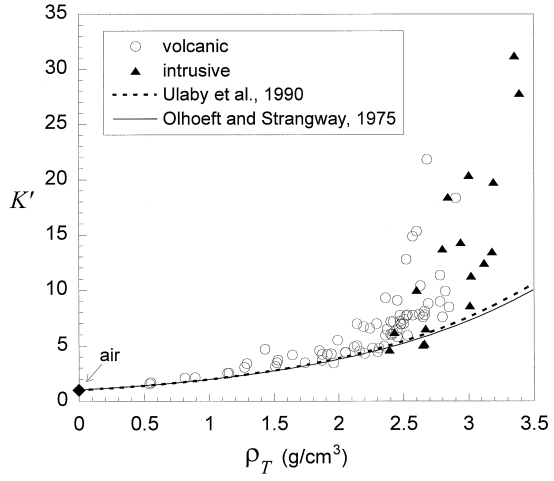

Fig. 1. Dielectric constant (K') is plotted against bulk density (ρ_T) for data from Shmulevich et al. (1971). Model curves (see text) derive from Ulaby et al. (1990) and Olhoeft and Strangway (1975).

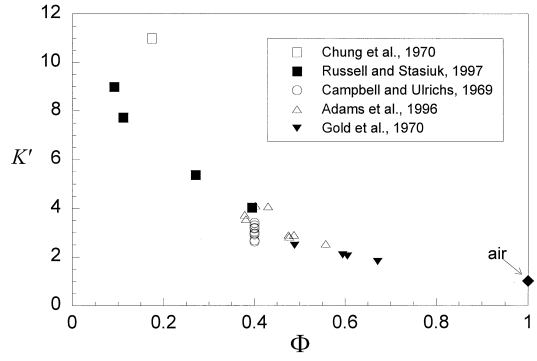

Fig. 2. Previously measured values of dielectric constant and porosity for volcanic rocks are plotted as K' vs. Φ. Legend includes sources.

titanium content (12 wt.% TiO_2). Porosity was calculated by examining the pore to rock ratio on the surface of the cylindrical sample. They assumed that this two-dimensional porosity was representative of the three-dimensional porosity (void volume over total volume) of the rock.

2.3. Effect of ilmenite on K'

Chung et al. (1970) attributed the higher dielectric constants of their lunar samples, relative to terrestrial basalts, to a greater ilmenite ($FeTiO_3$) content. Similarly, Hansen et al. (1973) found a positive correlation between dielectric constant and ilmenite content of some basalts. These findings are plausible as ilmenite has a dielectric constant of 30–80 (Parkhomenko, 1967; Nelson et al., 1989) compared to, for example, plagioclase, pyroxene and olivine which have dielectric constants between 4 and 11 (Keller, 1989; Nelson et al., 1989). However, neither Chung et al. (1970) nor Hansen et al. (1973) took into account relative porosities or densities of the samples. In fact, porosity data were reported for only one of the three samples examined by Chung et al. (1970). Olhoeft and Strangway (1975) compiled about ninety measurements for lunar rocks and soils and found no correspondence between K' and (TiO_2 + FeO) content when K' was normalized for constant bulk density. This result, however, does not necessarily negate ilmenite as one of the principal controls on dielectric properties of igneous rocks, because density also increases with increasing ilmenite content. A better understanding of the role of

Notes to Table 1:

[a]Additional parameters and physical properties: ρ, bulk density; Φ, porosity; X, composition (major oxides or mineral modes); (X), compositional data is published elsewhere; P, compressive pressure; T, temperature; $\tan\delta$, loss tangent or dielectric loss; σ, resistivity or conductivity; l_a, absorption length; R, reflectivity; p, polarization.

[b]Sources include: (1) Adams et al. (1996); (2) Bondarenko (1971); (3) Campbell and Ulrichs (1969); (4) Chung et al. (1970); (5) Drury (1978); (6) Frisnillo et al. (1975); (7, 8, 9) Gold et al. (1970); Gold et al. (1971); Gold et al. (1973); (10) Hansen et al. (1973); (11) Hawton and Borradaile (1989); (12) Howell and Licastro (1961); (13) Olhoeft and Strangway (1975); (14) Olhoeft et al. (1974); (15) Roberts and Lin (1997); (16) Russell and Stasiuk (1997); (17) Saint-Amant and Strangway (1970); (18) Shmulevich et al. (1971); (19) Shmulevich (1970); (20) Singh and Singh (1991); (21) Strangway et al. (1972); (22) Troitsky and Shmulevich (1973); (23) Tuck and Stacey (1978); (24) Ulaby et al. (1990).

[c]u, unconsolidated; s, solid; p, powdered.

[d]d, diameter; h, height; t, thickness.

[e]Assumed.

ilmenite would be gained by comparing rock compositions and modal mineralogies to values of K' normalized for porosity rather than density. The effects of other semiconducting oxides commonly occurring in volcanic rocks (magnetite and titanomagnetite) should also be considered.

3. Selection of sample suites

The central aim of this study is to explore the relationship between the porosity (or vesicularity) of volcanic rocks and their dielectric properties. We also elected to sample a variety of compositions of volcanic rocks in order to test for compositional controls on K'. Compositionally, the study suite spans dacite to basalt, and comprises: (1) dacite ($\sim$66–68 wt.% SiO_2) lava and pumice collected from lava flow, airfall and pyroclastic flow deposits, Mount Meager, B.C. (Stasiuk et al., 1996; Hickson et al., 1999); (2) dacite ($\sim$60–62 wt.% SiO_2) lavas from the Ring Creek lava flow, Garibaldi Volcanic Complex, (Sivertz, 1976; Brooks and Friele, 1992); (3) basalt ($\sim$51 wt.% SiO_2) from a Cheakamus Valley lava flow (Green, 1977; Nicholls et al., 1982; Higman, 1990); and (4) pahoehoe basalt ($\sim$49–50 wt.% SiO_2) lava from Mauna Ulu volcano (Swanson, 1973; Wright et al., 1974). Appendix A contains a compilation of the main mineralogical and chemical attributes of these volcanic rocks.

Hand samples were chosen in the field with the aim of maximizing the variance in vesicularity of samples from each deposit. This sampling scheme produced suites of rocks of similar composition and mineralogy with a spectrum of porosities (and bulk densities). Each hand-sample was cored, producing 5 cm diameter right cylinders. Bulk density (ρ_T) was calculated using measurements of weight, diameter and height. Samples that showed equal bulk densities from the same deposit were excluded from further procedures. From each core, a 0.5-cm-thick disk was prepared. In several instances, the cores showed large-scale textural heterogeneity, in which case multiple disks were prepared. For example, all five Mauna Ulu disks (each of which has a different porosity) derive from a single core. All disks were cleaned, dried in an oven at 105°C. Samples equilibrated with the room atmosphere for at least 2 days before physical properties were measured.

4. Measurement of porosity and density

In general, earlier studies of dielectric properties of volcanic rocks report values of bulk density (ρ_T) and not porosity. We have also measured ρ_T, which depends both on porosity and rock composition, in order to integrate our results with a larger data set from the literature. Density measurements are also used to cross-check primary porosity (Φ) measurements, by identifying samples with low apparent porosity due to unconnected pores.

4.1. Methods

Porosity was measured in two distinct ways. Firstly, porosity is calculated from measurements of volume:

$$\Phi = \frac{V_T - V_S}{V_T} \tag{5}$$

where V_T is the volume of the disk and V_S is the solid volume, excluding pores. Operationally, V_T is calculated geometrically on the basis of caliper measurements of height and diameter of the sample disks. V_S, on the other hand, is measured with a helium pycnometer, a technique based on the ideal gas law. If there are unconnected pores not accessed by the helium, then V_S is overestimated as it includes the unconnected pore volume. Therefore, this method of measurement yields the 'connected porosity' (Φ_{Conn}). The connected porosity is equal to 'total porosity' (Φ_T) only if all pores are connected.

The second way of determining Φ addresses the possibility that a fraction of the pores is not penetrated by helium during the pycnometer experiment. Φ_T as opposed to Φ_{Conn}, is calculated from:

$$\Phi_T = \frac{\rho_S - \rho_T}{\rho_S} \tag{6}$$

where ρ_T is the bulk density of the disk, and ρ_S is the density of the solid phase. The bulk density is determined by dividing the mass of the disks by their

Table 2
Measured values of bulk density (ρ_T), connected porosity (Φ_{Conn}), total porosity (Φ_T) and dielectric constant (K') for samples of volcanic rocks

Location	Sample	ρ_T	Φ_{Conn}	Φ_T	K'
Mount Meager	PM1a	1.083	0.528	0.575	3.411
	PM1b	1.086	0.529	0.573	3.429
	PM2a	0.937	0.543	0.623	3.073
	PM2b	0.807	0.589	0.675	2.795
	PM3	0.534	0.752	0.789	2.478
	PM5	0.710	0.675	0.715	2.689
	PM6	0.514	0.697	0.796	2.505
	PM8	0.688	0.691	0.723	2.703
	PM9	0.732	0.609	0.706	2.722
	PM10	0.603	0.651	0.758	2.498
	PF1	1.505	0.332	0.398	4.362
	MM1	2.377	0.075	0.083	6.074
	MM2	2.241	0.129	0.138	6.080
	MM3	2.142	0.175	0.180	5.341
	MM4	1.257	0.486	0.501	3.847
	MM5	1.454	0.408	0.417	4.366
	MB1	2.403	0.038	0.042	18.353
Ring Creek	RC1	2.320	0.122	0.130	6.372
	RC2	2.492	0.077	0.083	6.678
	RC3	2.419	0.093	0.099	6.493
	RC5	2.080	0.212	0.214	5.738
	RC6	1.788	0.318	0.313	5.161
	RC9	2.376	0.108	0.115	6.606
	RC10	2.207	0.164	0.165	5.984
	RC11	2.236	0.158	0.164	6.022
Mauna Ulu	ULUa	1.370	0.554	0.557	5.183
	ULUb	1.349	0.564	0.564	4.979
	ULUc	1.476	0.522	0.523	5.573
	ULUd	1.274	0.589	0.588	4.866
	ULUe	1.317	0.571	0.574	4.668
Cheakamus	CB5a	2.712	0.094	0.103	8.322
	CB5b	2.732	0.088	0.096	8.203
	CB7a	2.181	0.265	0.272	11.633
	CB7b	2.272	0.233	0.241	13.472

Dielectric constants are reported for a frequency of 10 MHz. Small letters indicate multiple disks from the same hand-sample.

volumes based on calliper measurements. The density of the solid phase, ρ_S is the void-free density of the sample disk. This measurement is made by crushing a portion of the hand-sample to 200 mesh and calculating the solid density from the mass of the powder and the He-pycnometer measured volume of the same sample of powder. Based on replicate measurements, the precision (1s) associated with measurements of ρ_S, ρ_T, Φ_{Conn} and Φ_T are all less than 1%.

4.2. Results

Measured values of bulk density, connected and total porosity are listed in Table 2. Fig. 3 is a comparison of the results of the two methods used to measure porosity. For porosities lower than 0.5, there is excellent agreement between Φ_T and Φ_{Conn} values. Sample PF1 represents a single notable exception ($\Phi_{Conn} = 0.33$, $\Phi_T = 0.40$). For porosities above 0.5, the measured total porosity is significantly greater than the connected porosity for many samples. The deviation ($\Phi_T - \Phi_{Conn}$) can be as large as 0.11. This indicates that there are unconnected pores in several disks and direct measurements using the helium pycnometer on solid samples may result in apparent porosities significantly lower than true porosities. In fact up to 17% of the pore space can be unconnected (e.g., sample PF1).

All samples showing differences in porosity values > 0.01 are from the Mount Meager suite of dacites. In thin section, these rocks are glassy and show a bimodal distribution of vesicles comprising large (mostly macroscopic), well-connected pores and small (< 0.25 mm), more poorly connected vesicles within the glassy matrix. In contrast, the Mauna Ulu basalts have porosities greater than 0.52 yet have virtually identical values of Φ_T and Φ_{Conn}. The implication is that all porosity is connected and in thin sections the samples of basalt show pores that are macroscopic and well-connected. Because both

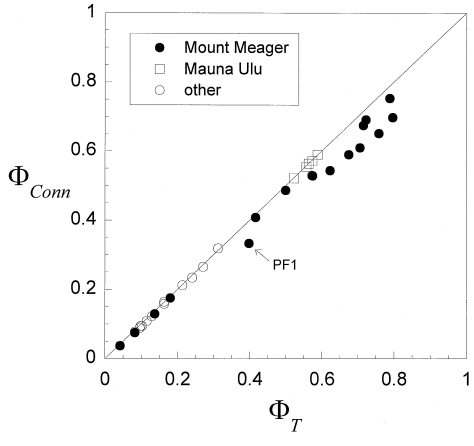

Fig. 3. Plot of values of connected porosity calculated from Eq. (5) vs. total porosity calculated from Eq. (6) for volcanic rock samples listed in Table 2. See text for details.

connected and unconnected pores should affect values of K', all subsequent references to sample porosities refer to total porosities as determined by Eq. (6).

Fig. 4a and b serve to illustrate, in another way, the importance of measuring Φ_T over Φ_{Conn}. For each rock suite of variable vesicularity and constant matrix, there should be a simple linear relationship between porosity and bulk density (Eq. (6)). Values of Φ plotted against ρ_T should produce a linear trend with y-intercept (Φ) of 1 and x-intercept (ρ_T) of ρ_S, the true density of the solid with no porosity.

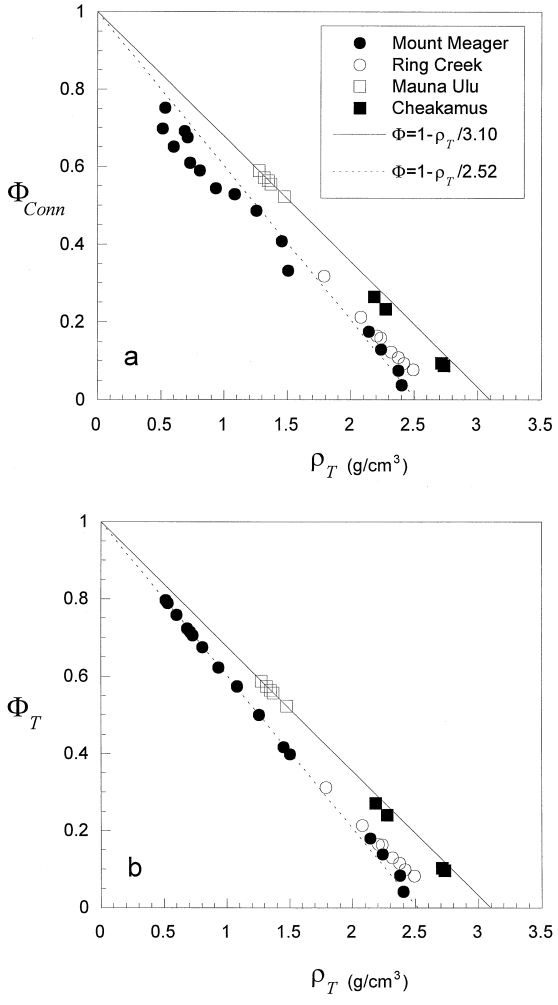

Fig. 4. Values of Φ_{Conn} (a) and Φ_T (b) are plotted against ρ_T. Measured values have been fit to model lines that extrapolate to values of solid density of 3.10 and 2.52 g/cm^3 (see text).

Different volcanic rock suites will have different x-intercepts because they have intrinsically different compositions and hence densities.

Fig. 4 develops this concept using values of Φ_{Conn} (Fig. 4a) vs. Φ_T (Fig. 4b). The data show significantly more scatter in Fig. 4a. In particular, plotted as Φ_{Conn}, the samples of dacite from Mount Meager are inconsistent with a straight line model suggesting different rock compositions. However, when the same data are plotted as Φ_T they fit a line of the form of Eq. (6). The Ring Creek suite forms a well-defined trend but, because most samples have low porosity, it does not extrapolate precisely to a y-intercept (Φ_T) value of 1 (corresponding to 100% air when the rock has no mass).

5. Measurement of K'

Capacitance data were collected with an HP4192A impedance analyzer using modified methods of Knight and co-workers in the Rock Physics Laboratory at the University of British Columbia (e.g., Knight and Nur, 1987; Knight and Abad, 1995). To make capacitance measurements, the dielectric material (rock) is placed between two parallel conductive plates (electrodes). Capacitance is a measure of the charge polarization that occurs in the sample between the plates. Dielectric constant (K') is the ratio of the capacitance with the dielectric material between the plates to the capacitance with a vacuum between the plates. Dielectric constant is calculated from capacitance (C) by:

$$K' = \frac{Cd}{\varepsilon_o A} \tag{7}$$

where A and d are the area and the separation of the electrodes, respectively, and ε_o is the permittivity of free space (8.554×10^{-12} F/m). Sample disks are approximately 5 cm in diameter and 0.5 cm thick. Dielectric constant data were collected at 25 frequencies over the interval 10 kHz to 10 MHz.

5.1. Experimental procedure

The standard procedure in the Rock Physics Laboratory at The University of British Columbia is to

form electrodes (capacitors) by sputtering gold on the top and bottom faces of the sample disks. This method could not be used in the present study because many of the samples are extremely porous (up to 80% pores) and/or contain large pores. Gold sputtering of the samples would have resulted in electrodes which deviated significantly from ideal parallel plates. The surface area of gold on a pumice sample, for example, would be much greater than the area calculated from the diameter of the disk. Also, the distance separating the electrodes would not be constant and in some cases would be substantially less than the height of the disk measured with callipers. Lastly, a few samples have pore networks which directly connect the upper and lower surfaces of the sample discs. Sputtering such samples may form a 'gold path' connecting the upper and lower electrodes rendering dielectric constant measurement impossible.

Several electrode configurations were tested on five samples having variable porosity, as well as on a non-porous material of known dielectric constant (STYCAST HiK; $K' = 6$). The different electrode forms included:

- 0.85-mm-thick copper disks;
- 0.025-mm-thick silver foil;
- silver paint on copper disks or silver foil;
- saline electrolyte-aqueous polymer gel (generally used to attach electrodes to skin) on copper disks or silver foil.

Where wet silver paint or gel was used to couple the copper disks or silver foil to the sample, it was applied to the metal rather than the rock to ensure an even distribution of paint and minimize the amount of conductive material entering pores. Prior to all measurements, the impedance analyzer was tested on a platinum-sputtered STYCAST HiK ($K' = 15$) disk with the same dimensions as the sample suite. Once placed in the sample holder and attached to the impedance analyzer, differences between repeated capacitance readings were insignificant for all electrode configurations tested.

The dielectric constant at low frequencies (below 10–100 kHz) was found to be extremely sensitive to the electrode configuration; however, at higher frequencies most methods converged to the same values of K'. Electrodes comprising copper disks or silver foil without Ag paint or gel as adhesive consistently produced the lowest values of K'. This is attributed to air gaps due to poor contact between the sample and the electrodes. When Ag paint was added (between sample and metal) higher dielectric constants were observed and using saline gel rather than Ag paint produced still higher values. Electrode configurations involving gel were rejected because measured values of K' for STYCAST HiK were always significantly higher than the reference value ($K' = 6$).

In the end, all data were collected using copper disks coupled to the sample with silver paint. We chose this method because: (1) the procedure generated consistent, reproducible results, (2) the copper discs are easier to handle than foil, and (3) the method reproduced the accepted value for the STYCAST HiK ($K' = 6$) standard to within 4% over the entire range of frequencies measured (10 kHz to 10 MHz). We also measured dielectric constant of four volcanic samples using silver foil in place of the copper disks; these two electrode configurations agree to within 1.4% at 10 MHz.

Although all samples were cored with the same bit, average disk diameters varied from $\sim$48 to 50.5 mm due to drill movement and contrasts in rock competency. Three pairs of copper disks of different diameters were made. The electrodes for each sample used the largest pair of copper disks whose diameter did not exceed that of the sample. The area used in Eq. (7) is the area of the copper disk rather than the sample area. The entire circular surfaces of six of the low porosity samples (MM1, MB1, RC2, RC9, CB5a, and CB5b) were coated with silver paint (no copper disks) and the entire area of the sample used in Eq. (7). In general, the dielectric constant determined using copper disks and silver paint is higher at lower frequencies and lower at higher frequencies than for silver paint alone (over the entire surface) but the deviation is less than 3% at 10 MHz except for a single outlier (MB1, $\sim$8% difference).

5.2. K'-frequency dependence

K' is a measure of polarizability and different polarization mechanisms dominate at different frequencies. The dominant mechanism at GPR frequencies is dipole polarization; at lower frequencies interfacial polarization (Maxwell–Wagner effect) can be

important. The latter mechanism occurs in heterogeneous materials and is caused by charge accumulations along interfaces when an electric field is applied (Howell and Licastro, 1961).

The measured values of dielectric constant for all samples are shown as a function of frequency in Fig. 5. Samples have higher dielectric constants at lower frequencies and decrease to a near-constant K' value at frequencies above 0.1–1 MHz. Notable exceptions are MB1 (a glassy clast from a welded block and ash dacite breccia), CB7a and CB7b (scoria from the base of a basalt lava flow), and to a lesser degree all Mauna Ulu samples (Fig. 5b). Samples MB1 and CB7a,b have significantly higher dielectric constants than other samples from the same deposits (Figs. 5 and 6a). Furthermore, for these samples, the measured values of K' do not level off at higher frequencies suggesting that the high values of K' reflect interfacial polarization, although this mechanism usually contributes little to K' in dry rocks. The Mount Meager outlier (MB1) has the same mineralogy as the rest of the Mount Meager suite but it is unique in that its pore spaces are almost exclusively in the form of cracks. It could be that the cracks host a thin ($\sim$ 10 Å) layer of adsorbed water, the presence of which has been shown to increase dielectric constant (Knight and Endres, 1990). A similar argument does not hold for the Cheakamus samples as the porosity is mainly in the form of primary vesicles.

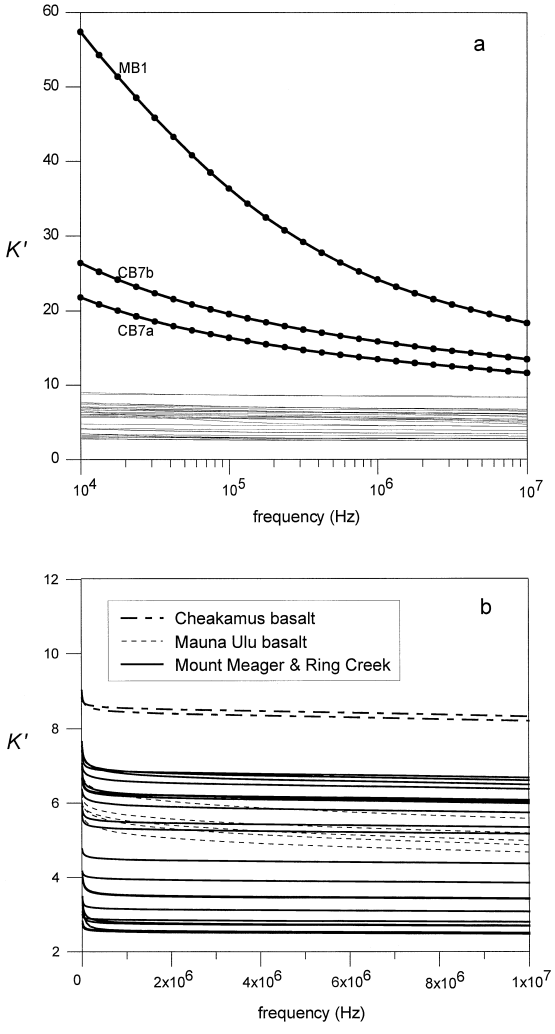

Fig. 5. Measured values of K' plotted as a function of frequency; K' was measured at the same 25 frequencies for all samples. (a) Data points (filled circles) are shown for samples MB1, CB7a and CB7b which have significantly higher dielectric constants and show greater frequency dependence than all other samples. (b) Samples with lower values of K' (<10) are plotted against a non-logarithmic frequency scale.

6. Relationship between Φ and K'

Comparisons of dielectric constant with porosity (Figs. 6a and 7) and bulk density (Fig. 8) are made with the highest frequency data (10 MHz). The suite with the most complete porosity spectrum is from Mount Meager. The data (excluding MB1) form a smooth and definite pattern in $K-\Phi_T$ space of increasing dielectric constant with decreasing porosity. The trend for Ring Creek data is approximately equivalent to that formed by the more felsic Mount Meager samples and, thus, the two suites are modeled as a single data set. The Mauna Ulu basalt samples show a similar pattern but define a distinct trend relative to the Mount Meager–Ring Creek (MM-RC) samples and are therefore treated separately. There are not enough Cheakamus basalt samples to form a coherent trend and these data were not modeled. Because the Mount Meager and Ring Creek suites span the greatest porosity, further discussion concentrates on this combined data set (excluding the outlier, sample MB1), henceforth referred to as the MM-RC data set.

A simple approach to modeling dielectric constant of a heterogeneous material is to calculate the total dielectric constant (K'_T) from the volume fraction (θ_i) and dielectric constant (K'_i) of each of the i components (e.g., pores vs. solids) using a model of the form:

$$(K^*_T)^\alpha = \Sigma\theta_i (K^*_i)^\alpha \quad (8)$$

where K^* is the complex dielectric constant and α is a geometrical factor. This is known as the equation of Lichtenecker and Rother (1931). The theoretical lower and upper limits of dipolar dielectric constant for a heterogeneous mixture occur where the components are arranged in series ($\alpha = -1$) and in parallel ($\alpha = 1$), respectively. When the components are non-conducting, K^* can be approximated by K' to yield:

$$(K'_T)^\alpha = \Sigma\theta_i (K'_i)^\alpha \quad (9)$$

This approximation is valid for our purposes because we treat our samples as mixtures of air (an insulator) and non-porous rock which is glassy or very fine-grained. As summarized in Appendix A, the total solid portions of our samples have very low abun-

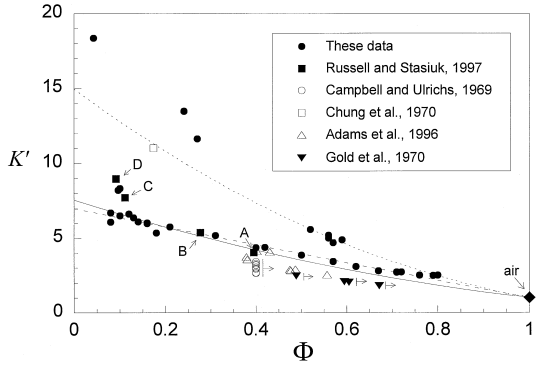

Fig. 7. Comparison of dielectric and porosity data sets from this study to previously published data. Porosity in this study represents total porosity whereas measurements from other sources may not be total porosity. Arrows attached to vertical lines indicate that porosities are minima but there is no significance to the arrow lengths. See text for details and explanations of labels. Model curves shown are identical to those in Fig. 6.

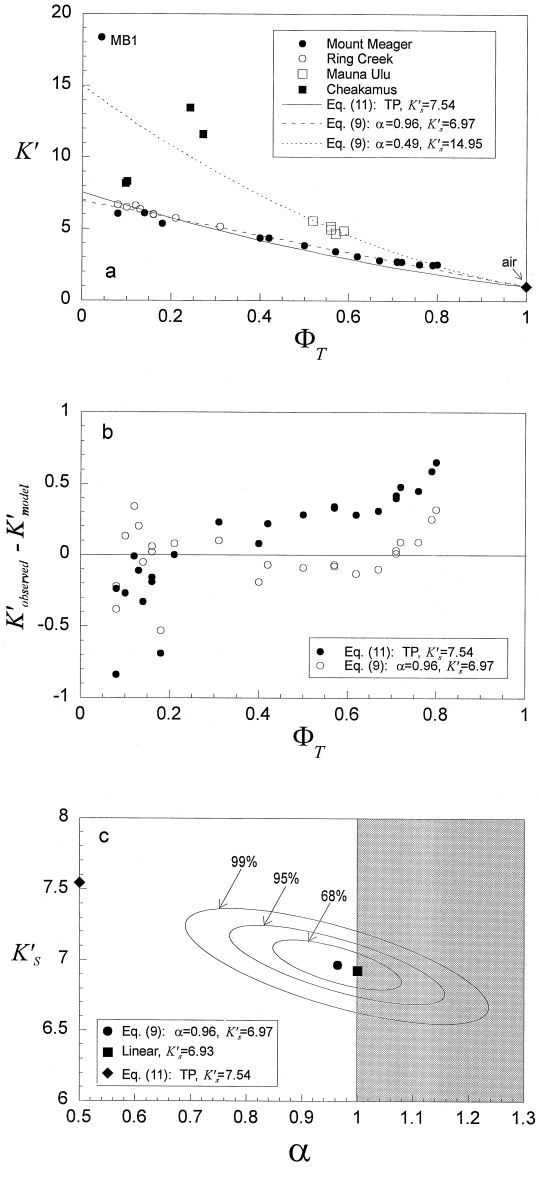

Fig. 6. (a) Experimental data from this study are plotted as K' vs. Φ and compared to model fitted curves, including: MM-RC data set fitted to TP model (Eq. (11), $K'_S = 7.54$); MM-RC data set fit to more general two-parameter model (Eq. (9), $K'_S = 6.97$, $\alpha = 0.96$); and Mauna Ulu data fit to two-parameter model (Eq. (9), $K'_S = 14.95$, $\alpha = 0.49$). (b) Plot of residuals on two fits to the MM-RC data set (e.g., Eqs. (9) and (11)). (c) Confidence limits on fit parameters K'_S and α (Eq. (9)) for MM-RC data set. The linear model (solid square) is also shown and is statistically equivalent to the two-parameter best-fit even at the 68% confidence level. The TP model solution ($\alpha = 0.5$) is also shown for comparison but lies outside solution space at the 99% confidence level. The shaded region represents physically unrealistic solutions for the dipolar dielectric constant of a heterogeneous mixture.

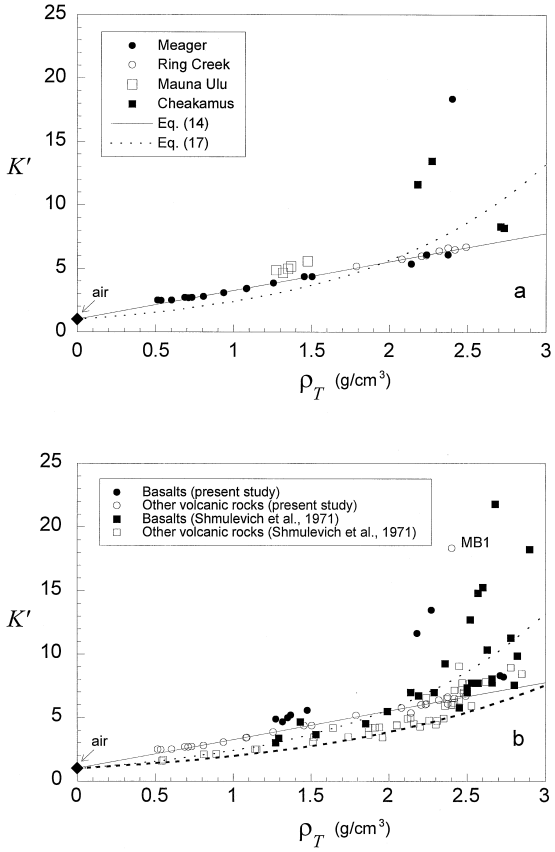

Fig. 8. Values of K' plotted against ρ_T. (a) These data are compared to two model curves fitted to the MM-RC data. Eq. (14) is a linear model constrained to pass through the value for air. Eq. (17) has the form used by Olhoeft and Strangway (1975) and Ulaby et al. (1990) (cf. Fig. 1). (b) Data from this study are compared to data on basalts and other volcanic rock types from Shmulevich et al. (1971). Heavy dashed line is model curve of Ulaby et al. (1990) shown in Fig. 1.

dances of conductive minerals (e.g., ilmenite) and, therefore, are essentially non-conductive.

A commonly used model of this type is the TP model (Wharton et al., 1980):

$$\sqrt{K'_T} = \Sigma \theta_i \sqrt{K'_1} \qquad (10)$$

In principle, one could build up the effective dielectric constant of a rock by taking into account the constituent minerals, glass, and air. Here, we consider each sample as a mixture of air ($K'_{air} = 1$) and a non-porous solid with a fixed dielectric constant K'_S, the expanded form of TP is:

$$\sqrt{K'_T} = \Phi_T + (1 - \Phi_T)\sqrt{K'_S} \qquad (11)$$

The general least squared-residuals best fit of Eq. (11) for the MM-RC data set gives $K'_S = 7.54$ (Table 3). This curve is plotted in Fig. 6a.

TP fits the MM-RC data well (Table 3); however, a plot of residuals (Fig. 6b) shows a systematic distribution. Part of this deviation from the model, particularly, the large residuals at high porosities, could be due to pore size and shape variation as TP does not take into account the geometry of the components. Alternatively, we have fit the data to Eq. (9) solving for both K'_S and α by minimization of the χ^2 function:

$$\chi^2 = \Sigma \frac{\left[K'_i - \left(K'(K'_S, \alpha)\right)\right]^2}{\sigma_i^2} \qquad (12)$$

(Press et al., 1986) where σ_i is the mean uncertainty on the measured values of K'_i. The optimal solution, $\alpha = 0.96$ and $K'_S = 6.97$:

$$(K'_T)^{0.96} = \Phi + 6.51(1 - \Phi) \qquad (13)$$

fits the data very well (Table 3, Fig. 6a). Furthermore, the residuals associated with this model show that the two parameter model is substantially better than the TP model for describing these data (Fig. 6b). Fig. 6c shows the 1s, 2s, and 3s (or 68, 95, 99%) confidence limits on the model solutions and demonstrates clearly that a TP model ($\alpha = 0.5$) lies outside the reasonable solution space. The α value for MM-RC data (0.96) is very close to the theoretical upper limit ($\alpha = 1$) which is strictly linear. A linear model constrained to pass through the theoretical value for air, has the fitted parameter $K'_S = 6.93$ (Table 3) and corresponds, in principle, to an arrangement of columns of rock and air perpendicular to the electrodes. Clearly, this is not an accurate

Table 3
Parameters to model lines describing K'-porosity data

Data set	Model	K'_S	α	R^2
MM-RC	TP: Eq. (11)	7.543	0.5[a]	0.979
MM-RC	Two-parameter fit: Eqs. (9) and (13)	6.965	0.965	0.985
MM-RC	Linear, through (0,1)	6.927	1[a]	0.984
Mauna Ulu	TP: Eq. (11)	14.768	0.5[a]	0.833
Mauna Ulu	Two-parameter fit: Eq. (9)	14.955	0.488	0.833

[a] Fixed value required by model.

description of the pore geometry of the entire MM-RC sample set. However, the Mount Meager pumice pores can be larger than, or of similar dimensions to, the thickness of the sample disks (0.5 cm), and the samples may be approaching a parallel arrangement at high porosities.

The Mauna Ulu basalt data were fit to the same models as the MM-RC data set (Table 3). TP (Eq. (11)) gives $K'_S = 14.77$ suggesting that the solid phase of the Mauna Ulu suite has a dielectric constant approximately double that of the Mount Meager and Ring Creek suites. The two-parameter fit (Eq. (9)) has optimal values $K'_S = 14.95$, $\alpha = 0.49$ which is essentially the same as TP ($\alpha = 0.5$) and is also plotted in Fig. 6a.

6.1. Comparison with previous results

Fig. 7 combines information from Figs. 2 and 6a by superimposing the new $K' - \Phi$ data on previous results. The data of Russell and Stasiuk (1997), labeled A through D, clearly agree with the data presented here, although Russell and Stasiuk (1997) used gold-sputtered surfaces as electrodes and only measured connected porosity. In particular, two samples of porous intermediate volcanic rocks (A and B) lie on the trend formed by Mount Meager and Ring Creek samples. Point D represents a sample of Cheakamus basalt from the same outcrop as sampled in this study. It plots relatively close to correlative samples in this study. These results indicate that the copper disks with silver paint electrodes give similar results to gold sputtering at low and moderate porosities. Point C is equivalent to the outlier MB1 of the present study but unlike MB1, its porosity is not dominated by cracks. The large gap in K' between samples C and MB1 is consistent with the abnormally high value for MB1 being related to its pore geometry.

The data from Campbell and Ulrichs (1969), Gold et al. (1970) and Adams et al. (1996) deviate from the trends defined by our data. There are several possible explanations for this disparity. Firstly, there are significant differences in rock composition. Secondly, the three previous studies measured K' on samples of powdered rock or natural ashes and, thus, the pore geometries would be substantially different from those found in the Mount Meager pumice samples. Thirdly, the porosities reported by Campbell and Ulrichs (1969) and Gold et al. (1970) are minima because it was assumed that the rocks from which the powders were crushed were non-porous. Finally, the data derived from the three previous studies were collected at much higher frequencies (450 MHz to 19 GHz vs. 10 MHz for the present study).

7. Relationship between ρ_T and K'

Plots of K' vs. total porosity (Fig. 6a) and K' vs. bulk density (Fig. 8a) are approximately mirror images of each other. This is not surprising as, for small variation in ρ_S, there is a simple relationship between porosity and bulk density (Eq. (6)). The basalts (Cheakamus and Ulu) have higher dielectric constants than the more acidic rocks (Mount Meager and Ring Creek) of similar porosity but the basalts also have higher ρ_S values (Fig. 4, Table 2). Bulk density is dependent on both Φ and ρ_S, and plotting K' vs. bulk density rather than porosity brings the data for basalt samples closer to the trend defined by MM-RC samples (Fig. 8a). However, the MM-RC and Ulu trends are still distinct in (ρ_T, K') space and only the MM-RC data set is modeled.

The MM-RC trend is remarkably linear (Fig. 8a). The best fit of a straight line constrained to pass through (0,1) is:

$$K' = 2.26\rho_T + 1 \quad (R^2 = 0.990) \tag{14}$$

Although the straight line fit is entirely empirical, it has two attributes: (a) it describes all of these data well (excluding MB1 and basalts), and (b) it offers a very simple model for making rapid estimates of K' for non-basaltic, dry, volcanic rocks based on a single measurement: ρ_T.

For the purposes of comparison, the MM-RC data were also fitted with a curve of the form used by Olhoeft and Strangway (1975) and Ulaby et al. (1990). Fits by Olhoeft and Strangway (1975) and Ulaby et al. (1990) relating K' to ρ_T data, are based on a logarithmic addition formula (Lichtenecker and Rother, 1931):

$$\log(K'_T) = \sum \theta_i \log(K'_i) \tag{15}$$

Treating the system as a mixture of air and non-porous rock, Eq. (15) simplifies to:

$$K'_T = K'^{(1-\Phi_T)}_S = K'^{\rho_T/\rho_S}_S \quad (16)$$

Assuming ρ_S is constant, K' can be related to ρ_T as was done by Olhoeft and Strangway (1975) and Ulaby et al. (1990) (Fig. 1). The resulting fit for the MM-RC data is:

$$K' = 2.22^{\rho_T} \quad (17)$$

This curve is plotted in Fig. 8a. The solution predicts higher K' for a given ρ_T than the models of Olhoeft and Strangway (1975) and Ulaby et al. (1990) (Eqs. (2) and (3)); however, the best fit to our experimental data is the linear model (Eq. (14)).

7.1. Comparison with previous results

Fig. 8b compares the (K', ρ_T) data from this paper to data for 68 volcanic rocks measured by Shmulevich et al. (1971) (e.g., Fig. 1). Plotted as K' vs. ρ_T, the present study shows higher K' for a given bulk density than most of the volcanic samples measured by Shmulevich et al. (1971) (Fig. 8b). This is particularly true at low bulk densities (high porosities). The most obvious and logical explanation for this disparity is the difference in measurement frequency (500 MHz vs. 10 MHz).

The data of Shmulevich et al. (1971) show a large spectrum of dielectric constants for basaltic rocks; indeed most of the dispersion in the $K' - \rho_T$ trend is due to basaltic samples (Fig. 8b). The number of basalts in the present sample set is limited. Although the Mauna Ulu samples show a clear trend of increasing dielectric constant with decreasing porosity, the span of porosities is too small to model accurately. Our Cheakamus basalts would not fit any air–rock mixing laws as the more porous samples (CB7a,b) from the base of the flow show much higher dielectric constants than the massive flow samples (CB5a,b). These anomalies may be a reflection of mineralogical variations. For example, the Cheakamus basalt samples have a high proportion of very-fine grained crystalline groundmass that contains higher abundances of Fe–Ti oxides than found in the glassy groundmass of the dacitic rocks (Table 4). Furthermore, although the overall content is low (< 7 wt.%), the basalt samples also show 2 to 3 times the normative contents of ilmenite and magnetite relative to the dacite samples (Table 5). In summary, excluding the basalt samples, our results parallel those of Shmulevich et al. (1971) and produce a single trend which can relate porosity or density to dielectric constant (Fig. 8b).

Table 4
Summary of ranges of modal mineralogy (vol.%) for samples used in this study

Unit	Mt. Meager[a]	Ring Creek[b]	Cheakamus[c]	Mauna Ulu[d]
Sample series	PM, PF, MM, MB	RC	CB	ULU
Rock type	dacite	dacite	basalt	basalt
Phenocrysts				
Olivine	–	–	6–8	< 5
Plagioclase	10–25	10–14	6–13	< 2
Pyroxene	3–10	–	–	< 2
Hornblende	3–5	–	–	
Fe–Ti oxide	1–4	–	–	
Groundmass				
Glass	60–80	20–31	4–11	85–90
Plagioclase	–	44–55	25–54	
Clinopyroxene	–	0–5	18–32	
Orthopyroxene	–	2–5	–	
Olivine	–	–	6–14	
Hornblende	–	0–4	–	
Fe–Ti oxide	–	4–6	3–6	

[a] Data are from this study and Stasiuk et al. (1996) and Hickson et al. (1999). Samples from this study with labels PM, PF, MM, and MB derive from deposits vtf, vpf, vd and vbx, respectively, of Stasiuk et al. (1996).
[b] Data are from this study or compiled from Sivertz (1976).
[c] Data taken from Green (1977), Nicholls et al. (1982), Lee (1988) and Higman (1990).
[d] Data are from this study. Lava is highly vesicular, contains sparse microphenocrysts and has a groundmass that comprises glass and subordinate amounts of undifferentiated microcrystalline quench crystals.

8. Applications and limitations of results for GPR

Volcanic deposits can show large variations in porosity that relate directly to process. Consequently, one of the attributes of this study is that we have established a clear relationship between Φ and K' for dry, non-basaltic volcanic rocks over a wide

Table 5
Representative chemical compositions (wt.%) for samples in this study and the corresponding calculated amounts (wt.%) of normative magnetite (Mt) and ilmenite (Il)

Unit	Mt. Meager				Ring Creek		Cheakamus	Mauna Ulu	
Label	PM-1	PF-1	MM-4	MB-1	RC-6	396-1	GV-7	70-1213 25	70-1213 62
Source	1	1	1	1	1	2	3	4	4
SiO_2	66.64	68.16	68.37	68.25	59.82	62.34	51.46	49.91	49.14
TiO_2	0.53	0.47	0.46	0.46	0.61	0.65	1.43	2.44	2.15
Al_2O_3	15.52	15.53	15.71	15.58	17.93	17.89	15.83	13.52	12.18
Fe_2O_3	–	–	–	–	–	2.11	1.44	1.39	1.15
FeO	3.53	3.05	3.08	3.05	4.56	3.26	8.71	10.07	10.62
MnO	0.09	0.08	0.09	0.08	0.11	0.10	0.14	0.18	0.17
MgO	1.95	1.30	1.31	1.30	2.36	1.52	7.38	8.55	12.02
CaO	3.51	3.26	3.33	3.25	5.18	5.79	8.45	10.85	9.86
Na_2O	4.51	4.59	4.63	4.63	4.15	4.24	3.70	2.27	1.98
K_2O	2.33	2.44	2.43	2.44	1.44	1.66	0.54	0.47	0.40
P_2O_5	0.16	0.15	0.15	0.15	0.32	0.48	0.23	0.23	0.21
H_2O/LOI	1.00	0.79	0.17	0.28	3.02	–	0.49	–	–
Total	99.77	99.82	99.73	99.47	99.50	100.04	99.80	99.88	99.88
Computed normative mineralogy									
Mt	0.46	0.49	0.49	0.49	0.74	3.06	2.09	2.02	1.67
Il	1.01	0.89	0.87	0.87	1.16	1.23	2.72	4.63	4.08
Total	1.57	1.38	1.36	1.36	1.90	4.29	4.81	6.65	5.75

Sources include: (1) This study; (2) Sivertz (1976); (3) Nicholls et al. (1982); (4) Wright et al. (1974).

range of porosities. The results indicate that inverse modeling techniques could be applied to GPR velocity data to derive estimates of porosities or map changes in porosity of dry volcanic deposits. One possible application is to map zones of welding in partially welded pyroclastic flows. The welded zones are composed of the same material as unwelded tops and bases but have lower porosity because slower cooling rates in the middle of the deposit provide sufficient time for hot clasts to flatten and thereby reduce porosity (e.g., Ross and Smith, 1961). If the change in porosity is gradational, a single, strong continuous reflection may not be generated (e.g., defining some critical porosity). However, by using CMP analysis, changes in velocity with depth could be determined and converted into a porosity profile.

Some caution should be taken in applying laboratory results directly to the interpretation of GPR data. Three main reasons are that: (1) the highest frequency used in these laboratory measurements is 10 MHz and this is significantly below conventional GPR frequencies for geological applications (e.g., 50–200 MHz), (2) there may be a problem in upscaling laboratory dielectric measurements on rock samples to the scale of deposits due to spatial heterogeneity (Chan and Knight, 1997), and most importantly, (3) in nature, the pore space may be partially saturated with water which could drastically alter the dielectric properties of a deposit because of the large contrast between K'_{water} (80) and K'_{air} (1).

We have treated volcanic rocks as binary systems consisting of nonporous rock and air. Whereas, the assumption that rocks are dry may be realistic in some climates, in general, it would be foolish to use our data to calculate porosity profiles from GPR data without assurance that the rocks are extremely dry (cf. Roberts and Lin, 1997). Further experiments with capacitance measurements made at a variety of water saturation levels (S_w) are required to develop a ternary empirical relationship describing the dielectric constant of wet volcanic rocks. For example, Roberts and Lin (1997) produced $K' - S_w$ data sets for three rhyolitic welded tuff samples. They used a measurement frequency of 100 kHz, whereas higher frequencies are required for models relevant to GPR applications because water enhances the frequency dependence of the data (e.g., Knight and Endres, 1990; Knoll and Knight, 1994).

Water can be accounted for using a theoretical mixing formula such as a TP model which has been found to work well for sedimentary rocks (Knoll and Knight, 1994). For example, using $K'_{rock} = 7.54$, $K'_{air} = 1$, and $K'_{water} = 80$, a TP model for the non-basaltic rock–air–water system is:

$$\sqrt{K'_T} = \sqrt{7.54}\,(1 - \Phi) + \Phi(1 - S_w) + \sqrt{80}\,\Phi S_w \quad (18)$$

where S_w is the fraction of pore space filled with water. If no water is present ($S_w = 0$), Eq. (18) reduces to an equation of the form of Eq. (11). The relationship expressed by Eq. (18) could be used to determine a porosity profile from GPR data, however, this requires a priori knowledge of S_w and, in general, actual S_w values are not known.

We advocate interpreting radar data in terms of relative velocities which can be used to map porosity patterns. This circumvents the potential inaccuracy of Eqs. (11) and (13) due to the presence of moisture. A higher porosity will still correspond to a higher velocity as long as the dielectric constant of the air–water mixture is less than that of the non-porous rock. Therefore, for values of water saturation that are less than about 20% and constant, relative porosity profiles could easily be determined with GPR. Particular caution is required in attributing decreasing velocity with depth to decreasing porosity because S_w commonly increases with depth in the vadose zone. Such a velocity pattern could correspond to a constant porosity with increasing fractions of the pore space filled with water down to the water table.

Although GPR has been used in geological studies since the 1960s, its application to problems associated with volcanic deposits is in its infancy. GPR will never replace traditional stratigraphic mapping but rather should complement it by extending observations of physical properties, distributions, thicknesses and internal structures to areas which lack exposure. In order to realize the full potential of GPR, a better understanding of the factors that contribute to the dielectric constant of volcanic rocks is paramount. The development of an empirical model relating porosity and dielectric constant of dry, non-basaltic volcanic rocks is an important step. Further work incorporating such factors such as mineralogy (e.g., ilmenite mode), pore and mineral geometries, and water content are required to enhance the simple models presented here.

Acknowledgements

Financial support for this research derives from NSERC Research Grant #OGP0820 (JKR) and an NSERC PGS A award (ACR). The manuscript was improved by critical reviews provided by Bruce Marsh and two anonymous reviewers.

Appendix A. Sample descriptions

The following tables are intended to provide a summary of the main petrographic (Table 4) and chemical (Table 5) characteristics of the rock samples used in this experimental study. The tables also list the primary sources which contain more complete descriptions of the volcanic rock units. The normative mineral abundances of ilmenite and magnetite (Table 5) are reported as wt.% values and were calculated using the reported FeO and Fe_2O_3 values or by assuming that Fe_2O_3 constituted 10% of the total iron content.

References

Adams, R.J., Perger, W.F., Rose, W.I., Kostinski, A., 1996. Measurements of the complex dielectric constant of volcanic ash from 4 to 19 GHz. J. Geophys. Res. 1, 8175–8185.

Bondarenko, A.T., 1971. Influence of high pressure and high temperatures on the dielectric constant of rocks of the Kola Peninsula. Earth Phys. 2, 92–96.

Brooks, G.R., Friele, P.A., 1992. Bracketing ages for the formation of the Ring Creek lava flow, Mount Garibaldi volcanic field, southwestern British Columbia. Can. J. Earth Sci. 29, 2425–2428.

Campbell, M.J., Ulrichs, J., 1969. Electrical properties of rocks and their significance for lunar radar observations. J. Geophys. Res. 25, 5867–5881.

Chan, C.Y., Knight, R.J., 1997. The transition zone between effective medium theory and ray theory for the propagation of electromagnetic waves. SEG Annual Meeting Expanded Technical Program Abstracts with Biographies, Vol. 67, pp. 422–425.

Chung, D.H., Westphal, W.B., Simmons, G., 1970. Dielectric properties of Apollo 11 lunar samples and their comparison with earth materials. J. Geophys. Res. 75, 6524–6531.

Drury, M.J., 1978. Frequency spectrum of the electrical properties

of seawater-saturated ocean crust and oceanic island basalts. Can. J. Earth Sci. 15, 1489–1595.

Frisnillo, A.L., Olhoeft, G.R., Strangway, D.W., 1975. Effects of vertical stress, temperature and density on the dielectric properties of lunar samples 72441,12, 15301,38 and a terrestrial basalt. Earth Planet. Sci. Lett. 24, 345–356.

Gold, T., Campbell, M.J., O'Leary, B.T., 1970. Optical and high-frequency electrical properties of the lunar sample. Science 167, 707–709.

Gold, T., O'Leary, B.T., Campbell, M., 1971. Some physical properties of Apollo 12 lunar samples. Proc. Second Lunar Sci. Conf. Geochim. Cosmochim. Acta, Suppl. 3, pp. 2173-2181.

Gold, T., Bilson, E., Yerbury, M., 1973. Grain size analysis and high frequency electrical properties of Apollo 15 and 16 samples. Proc. Fourth Lunar Sci. Conf. Geochim. Cosmochim. Acta, Suppl. 3, pp. 2149–2154.

Green, N.L., 1977. Multistage andesite genesis in the Garibaldi Lake area, southwestern British Columbia. PhD Thesis, University of British Columbia, Vancouver, Canada.

Hansen, W., Sill, W.R., Ward, S.H., 1973. The dielectric properties of selected basalts. Geophysics 38 (1), 135–139.

Hawton, M., Borradaile, G., 1989. Dielectric determination of rock fabric anisotropy. Phys. Earth Planet. Int. 56, 371–376.

Hickson, C.J., Russell, J.K., Stasiuk, M.V., 1999. Volcanology of the 2350 B.P. eruption of Mount Meager volcanic complex, British Columbia, Canada: implications for hazards from eruptions in topographically complex terrain. Bull. Volcanol. 60, 487–507.

Higman, S.L., 1990. Chemical discrimination of Cheakamus Valley basalt lava flows, southwestern British Columbia, statistical constraints. BSc Thesis, University of British Columbia, Canada.

Howell, B.F., Licastro, P.H., 1961. Dielectric behaviour of rocks and minerals. Am. Mineral. 46, 269–288.

Kanamori, H., Nur, A., Chung, D.H., Wones, D., Simmons, G., 1970. Elastic wave velocities of lunar samples at high pressures and their geophysical implications. Science 167, 726–728.

Keller, G.V., 1989. Electrical properties. In: Carmichael, R.S. (Ed.), Practical Handbook of Physical Properties of Rocks and Minerals. CRC Press, Boca Raton, FL, pp. 359–534.

Knight, R., Abad, A., 1995. Rock/water interaction in dielectric properties; experiments with hydrophobic sandstones. Geophysics 60, 431–436.

Knight, R.J., Endres, A., 1990. A new concept in modeling the dielectric response of sandstones: defining a wetted rock and bulk water system. Geophysics 55, 586–594.

Knight, R.J., Nur, A., 1987. The dielectric constant of sandstones, 60 kHz to 4 MHz. Geophysics 52, 644–654.

Knoll, M.D., Knight, R., 1994. Relationships between dielectric and hydrogeologic properties of sand–clay mixtures. Proc. Fifth Int'l Conf. on Ground Penetrating Radar, Kitchener, Ontario, June 1994, pp. 45–61.

Lee, L.J., 1988. Origin of columnar jointing in recent basaltic flows, Garibaldi area, southwest British Columbia. MSc thesis, University of Calgary, Calgary, Canada.

Lichtenecker, K., Rother, K., 1931. Deduction of the logarithmic Mixture law from general principles. Phys. Z. 32, 255–260.

Nelson, S.O., Lindroth, D.P., Blake, R.L., 1989. Dielectric properties of selected minerals at 1 to 22 GHz. Geophysics 54, 1344–1349.

Nicholls, J., Stout, M.Z., Fiesinger, D.W., 1982. Petrologic variations in Quaternary volcanic rocks, British Columbia, and the nature of the underlying mantle. Contrib. Mineral. Petrol. 79, 201–218.

Olhoeft, G.R., Strangway, D.W., 1975. Dielectric properties of the first 100 meters on the moon. Earth Planet. Sci. Lett. 24, 394–404.

Olhoeft, R.G., Frisnillo, A.L., Strangway, D.W., 1974. Electrical properties of Lunar Soil Sample 15301,38. J. Geophys. Res. 79, 599–1604.

Parkhomenko, E.I., 1967. Electrical Properties of Rocks. Plenum, New York, 314 pp.

Press, W.H., Flannery, B.P., Teukolsky, S.A., Vetterling, W.T., 1986. Numerical Recipes: The Art of Scientific Computing, 2nd edn. Cambridge Univ. Press, New York.

Roberts, J.J., Lin, W., 1997. Electrical properties of partially saturated Topopah Spring tuff: water distribution as a function of saturation. Water Resour. Res. 33, 577–587.

Ross, C.S., Smith, R.L., 1961. Ash-flow tuffs: their origin, geologic relations and identification. US Geol. Surv. Prof. Ap. 366, 77 pp.

Russell, J.K., Stasiuk, M.V., 1997. Characterization of volcanic deposits with ground penetrating radar. Bull. Volcanol. 58, 515–527.

Saint-Amant, M., Strangway, D.W., 1970. Dielectric properties of dry, geologic materials. Geophysics 35, 624–645.

Shmulevich, S.A., 1970. Determination of the dielectric characteristics of rocks in the wavelength range of 0.8–60 cm. Earth Phys. 19, 100–103.

Shmulevich, S.A., Troitskiy, V.S., Zelinskaya, M.R., Markov, M.S., Sukhanov, A.L., 1971. Dielectric properties of rocks at a frequency of 500 MHz. Earth Phys. 12, 68–76.

Singh, J., Singh, P.K., 1991. Studies of the dielectric constant of Indian rocks and minerals and some other materials. Pure Appl. Geophys. 135, 601–610.

Sivertz, G.W.G., 1976. Geology, petrology, and petrogenesis of Opal Cone and the Ring Creek lava flow. BSc thesis, University of British Columbia, Vancouver, Canada.

Stasiuk, M.V., Russell, J.K., Hickson, C.J., 1996. Distribution, nature, and origins of the 2400 BP eruption products of Mount Meager, British Columbia: linkages between magma chemistry and eruption behaviour. Geol. Surv. Can. Bull. 486, 27 pp.

Strangway, D.W., Chapman, W.B., Olhoeft, G.R., Carnes, J., 1972. Electrical properties of lunar soil dependence on frequency, temperature and moisture. Earth Planet. Sci. Lett. 16, 275–281.

Swanson, D.A., 1973. Pahoehoe Flows from the 1969–1971 Mauna Ulu Eruption, Kilauea Volcano, Hawaii. Geol. Soc. Am. Bull. 84, 615–626.

Troitsky, V.S., Shmulevich, S.A., 1973. Dependence of dielectric properties of rocks on their volume weight. J. Geophys. Res. 79, 6933–6935.

Tuck, G.J., Stacey, F.D., 1978. Dielectric anisotropy as a petrofabric indicator. Tectonophysics 50, 1–11.

Ulaby, F.T., Bengal, T.H., Dobson, M.C., East, J.R., Garvin, J.B., Evans, D.L., 1990. Microwave dielectric properties of dry rocks. IEEE Trans. Geosci. Remote Sensing 28 (3), 325–336.

Wharton, R.P., Hazen, G.A., Rau, R.N., Best, D.L., 1980. Electromagnetic propagation logging: advances in electromagnetic propagation logging. Soc. Petrol. Eng., AIME, Paper 9267.

Wright, T.L., Swanson, D.A., Duffield, W.A., 1974. Chemical composition of Kilauea east-rift lava 1968–1971. J. Petrol. 16, 110–133.